ADVANCING EARTH AND SPACE SCIENCE

Geophysical Research Letters

RESEARCH LETTER
10.1029/2021GL093543

Manifestations of Magnetotail Flow Channels in Energetic Particle Signatures at Low-Altitude Orbit

V. A. Sergeev[1], Weiqin Sun[2,3], Jian Yang[2], and E. V. Panov[4]

[1]Department of Earth Physics, St. Petersburg State University, St. Petersburg, Russia, [2]Department of Earth and Space Sciences, Southern University of Science and Technology, Shenzhen, China, [3]School of Atmospheric Sciences, Sun Yat-sen University, Zhuhai, China, [4]Institute of Physics, Karl-Franz University, Graz, Austria

Key Points:

- Strong step-like increases of energetic proton flux in the nightside auroral zone accompanied by depleted loss-cone of energetic electrons
- Such low-altitude spacecraft signatures were observed 12–14 min after flow burst passage over MMS in the near-conjugate plasma sheet
- RCM bubble simulation confirms such signature of azimuthal crossing of plasma bubble ionospheric projection and predicts its variability

Supporting Information:

Supporting Information may be found in the online version of this article.

Correspondence to:

V. A. Sergeev,
victor@geo.phys.spbu.ru

Citation:

Sergeev, V. A., Sun, W., Yang, J., & Panov, E. V. (2021). Manifestations of magnetotail flow channels in energetic particle signatures at low-altitude orbit. *Geophysical Research Letters*, *48*, e2021GL093543. https://doi.org/10.1029/2021GL093543

Received 25 MAR 2021
Accepted 8 JUL 2021

Abstract Although magnetotail bursty bulk flows (BBFs)/plasma bubbles are widely recognized as major plasma transport structures that provide particle acceleration and injection, their ionospheric signatures in energetic particles have not been established. In this study, we combine the ionospheric energetic proton flux (as a proxy to the equatorial pressure) and energetic electron loss-cone filling rate (as a marker of the equatorial magnetic field) to detect a rapid traversal from stretched to dipolarized field lines across the BBF channel. During a nonsubstorm episode when multiple flow bursts were observed in the plasma sheet, we show remarkable step-like increases of energetic proton flux (approaching 10^3 in some events) observed in the middle of nightside auroral zone. We also conduct a high-resolution Rice Convection Model (RCM) simulation of a plasma-sheet bubble intrusion into the inner magnetosphere. Besides confirmation of the observed signatures, the simulation illustrates variability of the ionospheric signatures of bubbles and provides guidance in future studies of flow burst interactions.

Plain Language Summary Flow bursts (also known as fast flow channels, or BBFs/bubbles) are sporadic transient narrow structures in the magnetotail which transport energy, and accelerate and inject energetic particles into the outer radiation belt and the ring current in the inner magnetosphere. Sparse spacecraft coverage severely limits experimental studies of such complicated structures and their flow braking process. For this purpose, an image of related precipitation on the ionospheric screen can be of great help if we could specify its magnetospheric context. In this study, we demonstrate a combination of two specific energetic particle signatures in the ionosphere to identify the border of BBFs. Sharp transition from isotropic to depleted loss-cone distributions of energetic electrons suggests the passage from stretched magnetic field lines outside the BBF to dipolarized lines inside the BBF. Sharp increase of energetic proton flux indicates the change of the equatorial pressure between stretched and dipolarized field lines. Observed together, these two signatures robustly indicate a sharp change in the magnetotail connectivity, a characteristic of BBFs. We also use the self-consistent numerical simulation of a plasma-sheet bubble injection to demonstrate these signatures on a physics-based model as well as to discuss the inherent variability of the signatures.

1. Introduction

The magnetotail fast flow bursts (Baumjohann et al., 1989) are widely known under different names, reflecting their different properties: the bursty bulk flows aka BBFs (Angelopoulos et al., 1992) reflecting their bursty appearance, fast flow channels (Nishimura et al., 2010) emphasizing narrow cross-tail size of fast flows, or the plasma-sheet bubbles (Chen & Wolf, 1993) defined using its lower flux-tube entropy than their neighbors. Besides being potentially important contributors to trigger and feed the magnetospheric substorm (Nishimura et al., 2010, 2014), they are widely recognized as major plasma transport vehicles in the magnetotail, capable of accelerating and injecting charged particles into the radiation belts and ring current (e.g., Birn & Hesse, 2013; Eshetu et al., 2019; Sorathia et al., 2018; Ukhorskiy et al., 2018; Yang et al., 2015). Investigations of BBFs/bubbles using magnetospheric spacecraft were very popular among researches during last two decades, providing a bulk of knowledge about their statistical properties, the characteristics of structures (e.g., Liu et al., 2013; Nakamura et al., 2004; Ohtani et al., 2004; Runov et al., 2015), the propagation and radial oscillations (e.g., Dubyagin et al., 2011; Panov et al., 2010; Runov et al., 2009, etc.).

However, BBFs/bubbles, which are localized and appear sporadically, may have a complicated geometry and travel a long distance in the tail (Runov et al., 2009). The research capabilities of existing magnetospheric observations are limited because of their episodic and sparse spacecraft coverage. Although the global MHD and kinetic drift models (e.g., Cramer et al., 2017; Wiltberger et al., 2015; Yang et al., 2011, 2019) have a large potential to simulate the bubbles in the realistic global environment and address important aspects of their physics, they have limitations. Currently, the global high-resolution simulations that include particle physics in realistic conditions are rare.

Deep understanding of several important aspects, including flow braking and formation of particle injection fronts, require a wider 2-D view of bubble development and its interaction with the ambient plasma. In these circumstances, the observations in the ionosphere or at low altitude have a great value, providing that (1) the ionospheric signatures of BBFs are identified reliably and (2) they help specify magnetospheric location of the observed structures. Currently, the mostly discussed signatures in the ionosphere include the auroral streamers and enhanced convection streams (see recent review by Forsyth et al. [2020]). However, when using them to identify and monitor the flow channel, one faces two problems.

One is that, whereas both aurora and convection are inherently structured due to action of different mechanisms (e.g., Karlsson et al., 2020), there is a paucity of tools to distinguish BBF-related structures from others. When using auroral observations alone, the identification of an auroral structure as an image of a BBF is easy if one can follow its development from poleward boundary of the oval toward its diffuse equatorward edge. This requires a global coverage of auroral dynamics—too rare an opportunity. If only local coverage is available, like that provided by a single ground ASI camera, often neither local arc orientation nor any other morphological details provide sufficient information to identify the arc as the BBF print. Particularly, the BBF-related streamers can develop either in north-south or in east-west directions (Zesta et al., 2006). In addition, an auroral streamer only displays the image of the duskward flank of a BBF, where the auroral electrons are accelerated in the upward field-aligned current (FAC). Correspondingly, neither the width of a BBF nor its shape transformation can be fully determined using auroral observations alone.

The other is that, neither of ionospheric observations provide markers to specify magnetospheric location of an observed structure. An interesting possibility exists to scan the equatorial B_Z distribution remotely using the low-altitude polar spacecraft, like Polar Operational Environmental Satellites (POES). Traversing the nightside auroral oval, the spacecraft can quickly scan the distribution of the loss-cone (LC) filling rate of energetic electrons in the plasma-sheet flux tubes, which is known to be dependent on magnetic field line curvature around the center of the current sheet (CS). Nonadiabatic scattering in the central CS leading to particle precipitation is well-known (see Delcourt et al., 1996; Sergeev et al., 1983). Summarizing briefly, the ratio of magnetic field line curvature radius (R_c) to the particle gyroradius (ρ) controls the average amplitude of pitch-angle (PA) change for the charged particle subpopulation characterized by the particle rigidity $G = mV/e$, where V is the total velocity of the particle. On the particle trajectory crossing the tail current sheet, the smallest R_c/ρ and largest scatter occur at the equatorial point where $R_c / \rho \approx B_Z^2 / \left(G\, d\sqrt{B_x^2 + B_y^2} / dz \right)$. Here if $R_c/\rho < 8$, the PA scattering is strong and entire loss-cone (LC) is filled isotropically during the traversal of current sheet. For $R_c/\rho > 8$, the scattering is weak and the loss-cone remains depleted. Correspondingly, for a given population (G), the critical point of transition from isotropic precipitation to depleted LC feature (known as isotropy boundary) implies a constraint on the value of equatorial B_Z on that field line, thereby providing the marker of the magnetotail location. For magnetotail applications, isotropy boundary of 40 keV protons has critical $B_Z \sim 40$–60 nT, being in the outer part of dipole-like region. For 40 keV electrons critical B_Z value is small, ∼5 nT (within a factor of 2, Sergeev, Gordeev, et al., 2018), thereby separating the current sheet domain ($B_Z < \sim 5$ nT) from dipolarized region ($B_Z \gg 5$ nT) which is of great value for our BBF-related study. For more discussion of this method and recent applications of remote sensing of the magnetotail from low altitudes see studies of the electron isotropy boundaries (Sergeev et al., 2012; Sergeev, Gordeev et al., 2018; Sergeev, Tsyganenko et al., 2018).

An additional marker could be the proton pressure or the energetic proton flux, as their values are nearly constant along the field lines in case of isotropic PA distributions formed in the plasma sheet (Wang et al., 2012) because of strong nonadiabatic PA scattering discussed above. In that case, the proton pressure/flux values observed at low-altitude spacecraft indicate their equatorial values in the current sheet, which

10.1029/2021GL093543

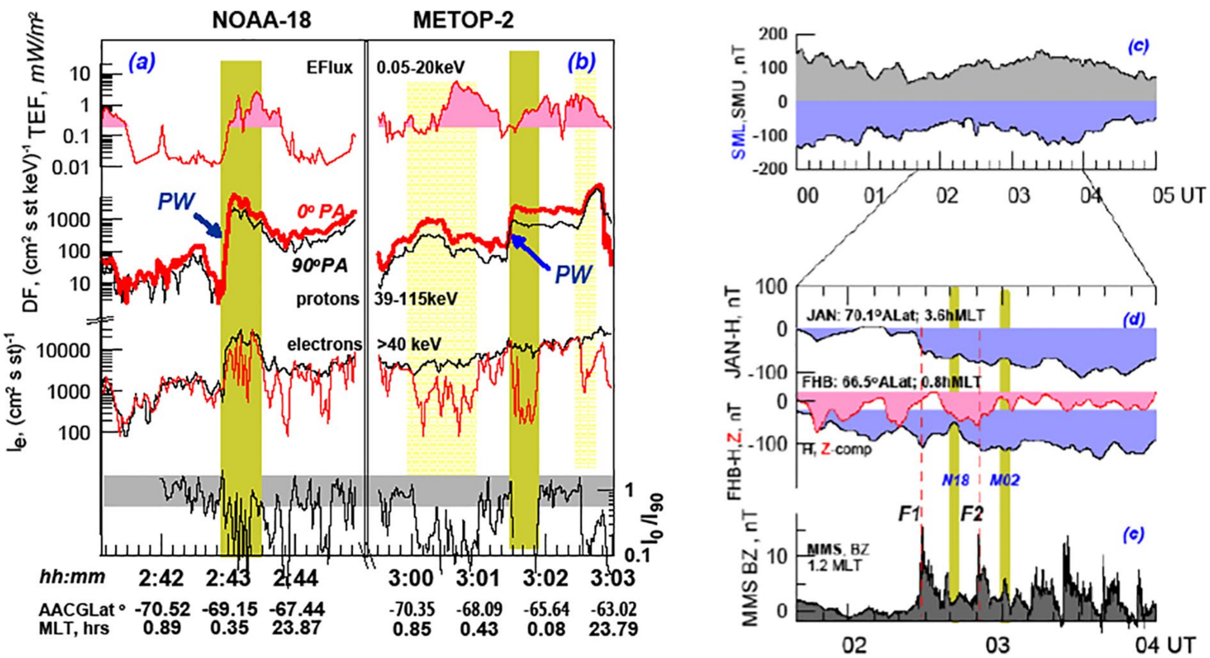

Figure 1. Summary of observations on June 14, 2018. Particle observations above southern auroral zone made by (a) NOAA-18 and (b) METOP-2 spacecraft; the ratio of precipitated (I_0) to trapped (I_{90}) flux of 40 keV electrons is shown in the bottom panels; (c) SuperMAG SMU and SML auroral electrojet indices; (d) *H*-component and *Z*-component magnetograms at stations FHB and JAN in near-midnight high-latitude part of the northern auroral zone (MLT is shown for 03:00 UT epoch); (e) B_Z magnetic variation measured at MMS in the conjugate plasma sheet.

strongly depend on the geocentric distance (Tsyganenko & Mukai, 2003). Previously there were only a few attempts of using this marker in the magnetospheric studies (Dubyagin et al., 2003; Kubyshkina et al., 2002).

Currently we are not aware of any previous systematic study of low-altitude BBF signatures in energetic particle data. This paper is motivated by the need to identify and investigate such signatures. To do this we combine two approaches. In Section 2, we show events in which spectacular variations in both energetic proton fluxes and in the loss-cone distributions of energetic electrons have been observed by POES spacecraft during the time when the BBFs were detected in nearly conjugate region of the tail plasma sheet. In Section 3, we employ the Rice Convection Model (RCM) simulation of an individual bubble injection to provide the global context between the ionospheric and magnetospheric manifestations of the bubble, and validate the low-altitude energetic particle signatures. In Section 4 we discuss the consistence between observations and modeling results, and the inherent variability of their signatures.

2. Observations

Low-altitude polar-orbiting POES-type satellites carry identical detectors to measure the total energy fluxes (TEF) of protons and electrons between 0.05 and 20 keV as well as energetic particle fluxes. In particular, they measure the proton energy fluxes between 39 and 115 keV as well as integral electron fluxes at >30 and >100 keV energies near-simultaneously inside and outside of the loss-cone at 2 s time resolution (Evans & Greer, 2000). The ratio of precipitated to trapped particle fluxes (I_0/I_{90}) provides a suitable diagnostic of the loss-cone filling rate.

During 02:00–04:00 h UT on June 14, 2018, two POES-type low-altitude polar spacecraft sequentially crossed the southern auroral zone near the midnight, first NOAA-18 (Figure 1a), and 20 min later METOP-2 (Figure 1b). Their trajectories were similar, moving from the postmidnight-poleward side to the premidnight-equatorward side of the auroral zone. Remarkably sharp increases of 39–115 keV proton fluxes were recorded at ∼02:43 and ∼03:02 UT, being located at −69.2° and −66.6° AACGM latitudes (Baker & Wing, 1989), respectively. The expanded views of particle measurements are available in Figures S1 and S2.

During the first event, NOAA-18 observed a spectacular increase of the energetic proton fluxed by a factor of 10^3 in only 8 s starting at 02:42:57 UT. During this short time, the NOAA-18 footpoint passed only 0.2° AACGLat and ~1° AACGLong in the ionosphere. During the second event observed by METOP-2, the flux increased stepwise by a factor of ~20 also within 8 s. The total energy flux of auroral protons between 0.05 and 20 keV (see Figures S1 and S2) displayed similar variations, but they were of smaller magnitude: the stepwise increases were only of a factor 2.4 and 4.4 for NOAA-18 and METOP-2, correspondingly. However, the upper panel of Figures 1a and 1b, reveals no sharp features with comparable magnitude in the auroral electron precipitation, sitting right on these proton flux structures. Motivated by step-like appearances of these features, by their large magnitude in energetic proton flux, as well as by relative weakness of accompanying electron flux variations, in the following we refer to them as the "proton (or pressure) wall" (PW) features.

In contrast to the protons, the energetic electrons behaved differently during the two crossings. In the first crossing (NOAA-18), the trapped e-flux at $E > 40$ keV (I_{90}) sharply increased by a factor of 10 (still much smaller than a factor ~10^3 for protons) and stayed at this level for about 20–25 s, which is 3 times longer compared to the PW duration. Before encountering PW, the precipitated e-flux (I_0) varied around the I_{90} flux level showing nearly isotropic loss-cone precipitation, as indicated by the I_0/I_{90} panel at the bottom of Figures 1a and 1b. When passing through the PW, the precipitated flux first increased together with the trapped flux. But it also displayed large fluctuations which look like a bursty precipitation (which could be caused by a resonant wave-particle interaction) superposed onto the empty loss-cone background. During the second crossing (METOP-2), there were no significant variations of the trapped electron flux across the PW but, again, the loss-cone suddenly depleted and remained so for 22 s. The loss-cone was filled isotropically both before and after the yellow strip, implying spacecraft transition from current sheet (low B_Z, isotropic electrons) to dipolarized plasma sheet (depleted LC feature) and back again. Here PW demarcates the eastward border of a wide depleted loss-cone region whose latitudinal width was about 0.7–0.8° latitude.

As regards the geomagnetic activity context, there was a modest convection activity without full-scale substorms during the first few hours of June 14, 2018, with the SME, SMU, and SML indices (SuperMAG analogs of standard AE, AU, and AL indices, Gjerloev, 2012) fluctuating around 200–300 nT SME level (Figure 1c). According to OMNI data (not shown) during the period of interest at 02:00–04:00 UT, the solar wind was slow (~310 km/s); the dynamic pressure was in the typical range (2.5–4 nPa); and a relatively steady interplanetary magnetic field had $B_Z \sim -1$ to -3 nT and $B_Y \sim -4$ nT. Persistent sporadic magnetic variations of ~100 nT amplitude were observed at stations situated in the poleward half of nightside auroral oval, in the sector where NOAA-18 and METOP-2 crossed the auroral zone. As illustrated by the records of stations JAN and FHB separated by ~2 h MLT (Figure 1d), these variations were relatively localized in longitude. Their time scales (10–15 min), location, and other properties are consistent with poleward boundary intensifications (PBI, after Lyons et al., 1999) which are known to be closely related to auroral streamers and magnetospheric BBFs (e.g., Forsyth et al., 2020; Zesta et al., 2002).

At 03:00 UT, the MMS spacecraft were at $X \sim -16$ Re and $Y \sim -5.5$ Re (i.e., at ~1.2 h MLT meridian, which is within 1 h MLT from the above discussed observations) and moved outward in the postmidnight plasma sheet. A series of BBFs were recorded at MMS between 02:00 and 04:00 UT (Figure 1e). In two most strong events, F1 and F2, accompanied by short-duration earthward flows of ~550 and ~360 km/s magnitude (not shown here), positive B_Z peaked at ~16 and 14 nT at 02:29 and 02:50 UT, respectively. The F1/F2 events preceded the low-altitude PW observations by 14 and 12 min, correspondingly. The association between the flow bursts and the PW events looks remarkable. If this is a causal relationship, the observed delay between PWs and flow burst passages implies that PW are related to some ~10 min delayed consequence of flow burst, rather than being caused directly by BBF passage throughout the plasma sheet.

Our interpretation of these observations is that each of two PWs were observed when POES crossed the dawnside bubble flank in the ionosphere, where a sharp change of magnetic connectivity between ionospheric and equatorial magnetic footprints occurred. Here the midtail flux tubes (having a weak plasma pressure and a small B_Z manifested in isotropic electron precipitation) may appear adjacent to the field lines coming from a BBF interaction region in the near tail (as shown by large pressure and B_Z, dipolarized region, empty loss-cone of energetic electrons). As previously discussed by Sergeev et al. (2004), see their Figure 6), strong change of connectivity, due to very different shapes of magnetic field lines inside and outside the bubble, is associated with a large magnetic shear (strong FAC sheet) observed at the BBF flanks. To test the feasibility of this scenario one has to address numerical simulation of the bubble in realistic magnetotail conditions, which will be the subject of the next section.

One may ask about the existence of auroral streamers during these episodes. By inspecting the precipitated total electron energy flux (upper trace in Figures 1a and 1b), one sees that electron precipitation is stronger on the right edge of dark yellow strips (at duskward BBF flank in our interpretation) as compared to its left side (on dawnward flank) as it should be in case of the BBF/bubble (Forsyth et al., 2020; Yang et al., 2011). From 20 to 30 s duration of yellow strips, we estimated the associated ionospheric scale-size along spacecraft trajectory to be 150–200 km. Taking into account that spacecraft trajectory could be tilted against the cross-track direction of-the flow channel, this size roughly corresponds to the width of streamer associated convective jet ~100 km (Gallardo-Lacour et al., 2014; Sergeev et al., 2004).

3. RCM Simulation

We simulate a generic bubble injection using the Rice Convection Model (RCM), which allows the calculation of the $E \times B$ and gradient/curvature drifts of both protons and electrons with isotropic distributions in 180 energy invariant channels. The recent improvement of the RCM includes the inertial effects, making it legitimate to model fast flow dynamics in the plasma sheet (Yang et al., 2019). The RCM is also two-way coupled with an MHD code (Silin et al., 2013), that is, the RCM provides plasma pressure to the MHD code and the MHD code provides the magnetic field to the RCM. We use a high grid resolution in this study, with 0.03° in latitude and 1.3° in longitude in the auroral zone; being mapped in the near-Earth plasma sheet, this corresponds approximately to 0.05 and 0.1 R_E in the X and Y directions.

Initial and boundary conditions are set up similar to previous RCM simulations (Yang et al., 2014). We use empirical T89 magnetic field model (Tsyganenko, 1989) equilibrated with a plasma pressure model (Lemon et al., 2003) driven by realistic solar wind parameters (IMF $B_Z = -3$ nT, number density $n = 14$ cm^{-3}, velocity $V = 310$ km/s) and geomagnetic index $K_p = 1$, from which the potential drop across the simulation region is estimated as 46 kV (Equation 12 of Zhang et al. [2009]). The plasma-sheet distributions in both the initial condition and the boundary condition are prescribed using an empirical model (Tsyganenko & Mukai, 2003), with the electron-temperature being 1/7 of proton temperature. For the first hour of the run, we simulate a substorm-growth-phase-like quasi steady convection, without bubble injections. At $T = 60$ min, we initiate the bubble at tailward boundary ($r \sim 18$ Re) by gradually decreasing the flux-tube entropy $PV^{5/3}$ (in 5 min) to 10% of that in the preinjection time in the region between 23.5 and 0.5 h in local time. For $T = 65$–70 min, $PV^{5/3}$ remains unchanged; and at $T = 70$ min, it begins to increase to the value of preinjection time within a duration of 5 min. After the recovery of $PV^{5/3}$, all parameters are held for 15 min until the end of simulation run. After launched from tailward boundary, the bubble develops earthward flow with its speed up to ~500 km/s at about $T = 70$ min. It eventually reaches ~6 R_E in the nightside. Movie S1 displays the differential flux of 39–115 keV protons and B_Z in both the equatorial plane and the ionosphere (mapped from the magnetosphere along the magnetic field lines with isotropic distribution assumption). The dipolarization peak (maximal equatorial B_Z change) is attained at $T \sim 71$ min, nearly coincident in both space and time with the peak values of proton flux. After $T = 71$ min, B_Z spreads slightly in local time and then gradually decreases.

Snapshots of equatorial distribution of 39–115 keV proton fluxes with overlaid contours of B_Z component (Figure 2a) and their ionosphere mapping along magnetic field lines (Figure 2b) are shown at $T = 71.3$ min. This epoch is roughly consistent with 12 min time delay of POES observations against the time when the bubble passed over MMS. Movie S1 and Figure 2 nicely show that regions of dipolarized B_Z and enhanced proton flux develop together. Their ionospheric mapping forms a remarkable poleward tongue, an ionospheric image of dipolarized region. In concert with picture of bubble development in the equatorial magnetotail, this tongue region grows poleward since $T = 65$ min during bubble propagation, reaching maximal development during the flow braking stage.

Three pink straight lines in Figure 2b represent trajectories of three virtual low-altitude satellite crossings, resembling trajectories of POES in Figure 1. Their mapped equatorial footpoints are also shown in Figure 2a. When the trajectories cross the tongue flank in the ionosphere, their equatorial footpoints display

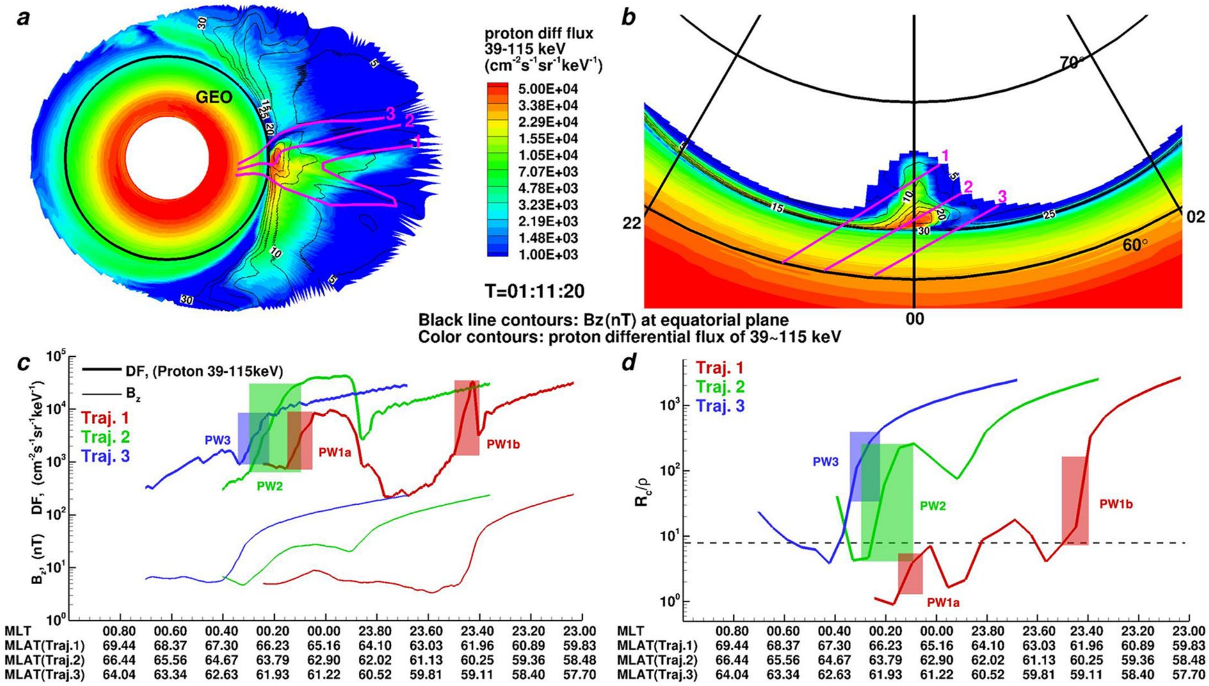

Figure 2. (a) Equatorial distribution of differential fluxes for 39–115 keV protons in color contours at $T = 71.3$ min. The black lines are contours of magnetic B_Z component. (b) Same quantities as (a), but plotted in the ionosphere by mapping along magnetic field lines. The three pink straight lines in (b) represent virtual satellite trajectories in the ionosphere; their mapped equatorial footprints are also plotted in panel (a). (c) Logarithm scale plot of proton differential flux (thick lines) and magnetic B_Z component (thin lines) along three trajectories shown in panel (a). (d) Logarithm scale of $R_c\ /\ \rho$ for 40 keV electrons for the same satellite trajectories. The colored rectangles mark the time interval of major increases of the proton flux.

rapid and large earthward displacement, manifesting rapid change of connectivity between the ionosphere and magnetosphere which occurs on short segments of the trajectory. (For example, for trajectory 2 the equatorial footpoint displacement from 16 to 7.2 Re occurred when the latitude changed only by 1° and longitude by 5°).

Figure 2c shows the proton flux and B_Z variations along three trajectories. Each trajectory demonstrates large step-like increases of proton flux labeled as PW1a/b, PW2, PW3. Usually these increases accompany the step-like B_Z increases. They are associated with sharp connectivity changes. The peak flux connects to the inner magnetosphere where largest proton flux (also the largest B_Z and proton pressure) are available. In the largest event PW2, proton flux increased by a factor ~70, which looks similar to NOAA-18 observations in Figure 1a, though with smaller magnitude. The event PW1a looks different: its poleward most trajectory crossed the top of tongue, and its equatorial projection did not map closer than 10 Re resulting in relatively weak increase of associated B_Z.

The energetic electron precipitation cannot be directly modeled in the RCM, due to its isotropic assumption. However, the expectation of whether the charged particle can be scattered nonadiabatically into the loss-cone (when $R_c/\rho < 8$), or the loss-cone will stay depleted (when $R_c/\rho > 8$) can be predicted based on self-consistently computed magnetic field. As shown in Figure 2d, initially for three virtual spacecraft R_c/ρ is near (trajectories 2, 3) or below (trajectory 1) that threshold for 40 keV electrons and here an isotropic precipitation from the midtail can be expected. Close to the time of BBF flank crossing R_c/ρ jumps above the threshold as a consequence of B_Z increase for trajectories 2, 3. Whereas the absolute magnitudes of B_Z and R_c/ρ may be somewhat different between the presented event and the bubble simulation, general association of proton wall with transition from isotropic to depleted loss-cone distribution of energetic electrons looks as natural manifestation of the bubble flank in the ionosphere.

Simulation results demonstrate some variability of the energetic particle signatures associated with the BBF/bubble. For example, B_Z (and R_c/ρ) variation in the most poleward crossing PW1a is insufficient and

10.1029/2021GL093543

the change of electron loss-cone filling regime may not be detected. Or, R_c/ρ (B_Z related) small variations around the threshold between 23.8 and 23.6 MLT on trajectory 1 may cause alternating changes of electron anisotropy, without accompanying proton flux variations. This occurs in the middle of BBF structure and may reflect some internal structure of the bubble. This episode also shows a limitation of electron-based remote sensing, which has a threshold nature and does not indicate the amplitude of B_Z variation unless a few different energy channels are used.

On the other hand, in association with variations PW3 and PW1b, B_Z increases stepwise to high values typical for a geostationary orbit. From Figure 2b, we see that these cases represent an entry to the inner region on the duskside (and dawnside) from the BBF-related tongue. Such events are not uncommon in observations too. Figure 1b shows such an example starting at 03:02:30 UT (light yellow-shaded strip). These events may rather represent crossings of azimuthally aligned narrow interface (magnetic wall) between earthward convecting plasma sheet and dipole-like inner region, which has been detected in RCM simulations at the end of the growth phase (Yang et al., 2013) and also in association with the bubble intrusion (Yang et al., 2014). Therefore, such events may not be exclusively related to the crossing of the bubble itself. They are easily distinguished from bubble crossings by their proximity to proton isotropy boundary and electron signature of the radiation belt (these boundaries are marked in Figures S1 and S2).

How long could the bubble signatures be observed after the bubble intrusion? The simulation shows that the dipolarization-related tongue grows to its peak after 11 min of its initiation from −18 Re (see Movie S1). Then it relaxes slowly so that 20 min later, at the end of simulation run, the tongue remnant could still be seen. Such timescale of a few tens minutes was previously inferred for the relaxation of plasma pressure observed in front of a stopping BBF/bubble (Sergeev et al., 2014), and for the relaxation of integral field-aligned currents after simulated bubble events (Birn & Hesse, 2013). From that we may expect that dipolarization effects produced by the bubble, may be seen at a later stage of its intrusion as well as during the subsequent 10–20 min, although with a smaller probability. This is consistent with observed time delays presented in Figure 1.

4. Discussion and Concluding Remarks

In this paper, we show observations and RCM simulation results to argue that sudden increase of energetic proton flux and change from isotropic precipitation to depleted loss-cone distribution of energetic electrons may serve as a signature to detect the BBF/bubble in the ionosphere. Its prints are detectable for 10–20 min after the bubble intrusion. For the first time, we show examples of spectacular step-like proton flux increases (proton flux wall, "PW" events) and emphasize their importance as markers of regions where sharp change of ionosphere-magnetosphere connectivity can occur. Our quick inspection of POES observations for other periods indicated that such PW events are not uncommon during both substorm and nonsubstorm times.

Temporal transitions between the isotropic and depleted LC distributions of electrons can be related to the crossing of dipolarized flux tubes, which may have various shapes and orientations, and stay at any distance in the tail. However, its combination with large sharp proton flux change appears to be a distinctive property of radially elongated flow channel, whose one end intrudes into the high-pressure (and large Bz) interaction region in the inner magnetosphere while the other end resides in the midtail. Thus, the combination of two observations available on POES spacecraft makes interpretation more straightforward and reliable. Minimal and maximal proton counts at PW can serve as pressure markers corresponding to distant and near-Earth parts of the encountered part of flow channel.

There arises the question—could there be other ways to explain large proton flux differences in nearby points in the ionosphere? This problem has a few aspects. Normally the plasma sheet is in pressure balance with the lobes where the radial and azimuthal pressure gradients are small in the tail. This may possibly be violated during sharp temporal variations (e.g., explosive reconnection), or during fast propagation of compact structures, like BBFs, dipolarization fronts, flux ropes, etc. The BBF-related changes are most well studied in observations. Comparing parameters observed on two sides of an earthward propagating BBF front, Runov et al. (2015) found that, on average, Ti is about 40% higher inside BBF than outside and that, due to a density decrease, the proton pressure variation is small. The increase of >30 keV proton flux constitutes about two-times across the BBF front, with no indications of much larger increases in individual events, which are comparable to changes at PWs shown in Figure 1.

As regards temporal variations, Kauristie et al. (2003) reported a 30% enhancement of the proton energy flux by observing variations of H-β emission just at the time and in the location where the equatorward end of the streamer reached the H-β band. Simultaneously they observed poleward shift of the H-β emission region suggesting magnetic field dipolarization in equatorial magnetosphere. About two-fold increase of the peak plasma pressure was reported in front of stopping BBF in observations (Sergeev et al., 2014) as well as in the bubble simulations (Birn & Hesse, 2013; Yang et al., 2011). It seems that both the equatorial pressure and proton energy flux in the magnetotail are rather conservative in association with bubble interactions as well as during substorms. For example, its peak value increases by only a factor of 2 under the substorm initiation region (Mende et al., 2003).

One more aspect of the problem, which is not modeled in the RCM, is that fast transient earthward flow contains significant field-aligned component. Particularly, an off-equatorial high-pressure region forms and propagates earthward along the field line (Birn et al., 2004; Chen & Wolf, 1999; Ebihara & Tanaka, 2015). It particularly manifests in the difference between the ionospheric and equatorial pressure values in the same flux tube, which has a different sign at different phases of bouncing pressure evolution. Establishing a full equilibrium may take many Alfvén transit times (Birn et al., 2004). It is encouraging that above discussed pressure differences were rather modest, with the pressure differences or variations in most cases being within a factor of 2–3. In summary, this brief discussion shows that there is no obvious mechanism, other than sharp connectivity change at the bubble borders, which is capable to generate changes of the energetic proton flux as large as a factor 20 to 1,000 in the nearby points of the ionosphere, as shown in Figures 1a and 1b.

Note that usefulness of low-altitude energetic particle diagnostics would increase significantly with higher spectral resolution of the energetic electron instrument and, especially, when complementary auroral observations are available, because optical observations provide information about structures orientation, spatial pattern, and dynamical context. Such combination would be invaluable in addressing (among others) the long-standing problems of flow braking, energetic particle injection, and the bubble interactions with the inner magnetosphere in general.

Data Availability Statement

The RCM simulation output can be accessed through https://zenodo.org/record/4603483#.YE2-H50zYZ2.

Acknowledgments
POES and MMS spacecraft observations as well as ground magnetograms used in this paper are available via CDAWeb site (http://cdaweb.gsfc.nasa.gov). SMU/SML auroral indexes are provided by SuperMAG project (https://supermag.jhuapl.edu/), the authors gratefully acknowledge the SuperMAG collaborators. The energetic particle analyses (work in SPbU) were supported by Russian Ministry of Science and High Education grant N075-15-2021-583. E. V. Panov acknowledges the support by the Austrian Science Fund (FWF): I 3506-N27. The work at SUSTech was supported by grant 41974187 of the National Natural Science Foundation of China (NSFC) and grant XDB41000000 of the Strategic Priority Research Program of the Chinese Academy of Sciences. This paper initiated from discussions while establishing the international team "Magnetotail Dipolarizations: Archimedes Force or Ideal Collapse? " supported by the International Space Science Institute (ISSI) in Bern.

References

Angelopoulos, V., Baumjohann, W., Kennel, C. F., Coroniti, F. V., Kivelson, M. G., Pellat, R., et al. (1992). Bursty bulk flows in the inner central plasma sheet. *Journal of Geophysical Research*, *97*(A4), 4027–4039. https://doi.org/10.1029/91JA02701

Baker, K. B., & Wing, S. (1989). A new magnetic coordinate system for conjugate studies at high latitudes. *Journal of Geophysical Research*, *94*(A7), 9139–9143. https://doi.org/10.1029/JA094iA07p09139

Baumjohann, W., Paschmann, G., & Cattell, C. A. (1989). Average plasma properties in the central plasma sheet. *Journal of Geophysical Research*, *94*(A6), 6597–6606. https://doi.org/10.1029/JA094iA06p06597

Birn, J., & Hesse, M. (2013). The substorm current wedge in MHD simulations. *Journal of Geophysical Research: Space Physics*, *118*, 3364–3376. https://doi.org/10.1002/jgra.50187

Birn, J. M., Raeder, J., Wang, Y. L., Wolf, R. A., & Hesse, M. (2004). On the propagation of bubbles in the magnetotail. *Annales Geophysicae*, *22*, 1773–1786. https://doi.org/10.5194/angeo-22-1773-2004

Chen, C. X., & Wolf, R. A. (1993). Interpretation of high-speed flows in the plasma sheet. *Journal of Geophysical Research*, *98*(A12), 21409–21419. https://doi.org/10.1029/93JA02080

Chen, C. X., & Wolf, R. A. (1999). Theory of thin-filament motion in Earth's magnetotail and its application to bursty bulk flows. *Journal of Geophysical Research*, *104*(A7), 14613–14626. https://doi.org/10.1029/1999JA900005

Cramer, W. D., Raeder, J., Toffoletto, F. R., Gilson, M., & Hu, B. (2017). Plasma sheet injections into the inner magnetosphere: Two-way coupled OpenGGCM-RCM model results. *Journal of Geophysical Research: Space Physics*, *122*, 5077–5091. https://doi.org/10.1002/2017JA024104

Delcourt, D. C., Sauvaud, J.-A., Martin, R. F., Jr., & Moore, T. E. (1996). On the nonadiabatic precipitation of ions from the near-Earth plasma sheet. *Journal of Geophysical Research*, *101*(17), 17409–17418. https://doi.org/10.1029/96JA01006

Dubyagin, S., Sergeev, V., Apatenkov, S., Angelopoulos, V., Runov, A., Nakamura, R., et al. (2011). Can flow bursts penetrate into the inner magnetosphere? *Geophysical Research Letters*, *38*, L08102. https://doi.org/10.1029/2011GL047016

Dubyagin, S. V., Sergeev, V. A., Carlson, C. W., Marple, S. R., Pulkkinen, T. I., & Yahnin, A. G. (2003). Evidence of near-Earth breakup location. *Geophysical Research Letters*, *30*(6), 1282. https://doi.org/10.1029/2002GL016569

Ebihara, Y., & Tanaka, T. (2015). Substorm simulation: Insight into the mechanisms of initial brightening. *Journal of Geophysical Research: Space Physics*, *120*, 7270–7288. https://doi.org/10.1002/2015JA021516

Eshetu, W. W., Lyon, J. G., Hudson, M. K., & Wiltberger, M. J. (2019). Simulations of electron energization and injection by BBFs using high-resolution LFM MHD fields. *Journal of Geophysical Research: Space Physics*, *124*, 1222–1238. https://doi.org/10.1029/2018JA025789

Evans, D. S., & Greer, M. S. (2000). *Polar orbiting environmental satellite space environment monitor-2: Instrument descriptions and archive data documentation (NOAA Technical Memorandum, OAR SEC version 1.4*, Vol. 93). NOAA.

Forsyth, C., Sergeev, V. A., Henderson, M. G., Nishimura, Y., & Gallardo-Lacourt, B. (2020). Physical processes of meso-scale, dynamic auroral forms. *Space Science Reviews*, *216*, 46. https://doi.org/10.1007/s11214-020-00665-y

Gallardo-Lacourt, B., Nishimura, Y., Lyons, L. R., Zou, S., Angelopoulos, V., Donovan, E., et al. (2014). Coordinated SuperDARN THEMIS ASI observations of mesoscale flow bursts associated with auroral streamers. *Journal of Geophysical Research: Space Physics*, *119*, 142–150. https://doi.org/10.1002/2013JA019245

Gjerloev, J. W. (2012). The SuperMAG data processing technique. *Journal of Geophysical Research*, *117*, A09213. https://doi.org/10.1029/2012JA017683

Karlsson, T., Andersson, L., Gilies, D. M., Lynch, K., Marghitu, O., Paramies, N., et al. (2020). Quiet, discrete aurora arcs: Observations. *Space Science Reviews*, *216*. https://doi.org/10.1007/s11214-020-0641-7

Kauristie, K., Sergeev, V. A., Amm, O., Kubyshkina, M. V., Jussila, J., Donovan, E., & Liou, K. (2003). Bursty bulk flow intrusion to the inner plasma sheet as inferred from auroral observations. *Journal of Geophysical Research*, *108*(A1), 1040. https://doi.org/10.1029/2002JA009371

Kubyshkina, M. V., Sergeev, V. A., Dubyagin, S. V., Wing, S., Newell, P. T., Baumjohann, W., & Liu, A. T. Y. (2002). Constructing the magnetospheric model including pressure measurements. *Journal of Geophysical Research*, *107*(A6). SMP 4-1–SMP 4-9. https://doi.org/10.1029/2001JA900167

Lemon, C., Toffoletto, F., Hesse, M., & Birn, J. (2003). Computing magnetospheric force equilibria. *Journal of Geophysical Research*, *108*(A6), 1237. https://doi.org/10.1029/2002JA009702

Liu, J., Angelopoulos, V., Runov, A., & Zhou, X.-Z. (2013). On the current sheets surrounding dipolarizing flux bundles in the magnetotail: The case for wedgelets. *Journal of Geophysical Research: Space Physics*, *118*, 2000–2020. https://doi.org/10.1002/jgra.50092

Lyons, L. R., Nagai, T., Blanchard, G. T., Samson, J. C., Yamamoto, T., Mukai, T., et al. (1999). Association between Geotail plasma flows and auroral poleward boundary intensifications observed by CANOPUS photometers. *Journal of Geophysical Research*, *104*(A3), 4485–4500. https://doi.org/10.1029/1998JA900140

Mende, S. B., Frey, H. U., Morsony, B. J., & Immel, T. J. (2003). Statistical behavior of proton and electron auroras during substorms. *Journal of Geophysical Research*, *108*(A9), 1339. https://doi.org/10.1029/2002JA009751

Nakamura, R., Baumjohann, W., Mouikis, C., Kistler, L. M., Runov, A., Volwerk, M., et al. (2004). Spatial scale of high-speed flows in the plasma sheet observed by Cluster. *Geophysical Research Letters*, *31*, L09804. https://doi.org/10.1029/2004GL019558

Nishimura, Y., Bortnik, J., Li, W., Lyons, L. R., Donovan, E. F., Angelopoulos, V., & Mende, S. B. (2014). Evolution of nightside subauroral proton aurora caused by transient plasma sheet flows. *Journal of Geophysical Research: Space Physics*, *119*, 5295–5304. https://doi.org/10.1002/2014JA020029

Nishimura, Y., Lyons, L., Zou, S., Angelopoulos, V., & Mende, S. (2010). Substorm triggering by new plasma intrusion: THEMIS all-sky imager observations. *Journal of Geophysical Research*, *115*, A07222. https://doi.org/10.1029/2009JA015166

Ohtani, S., Shay, M. A., & Mukai, T. (2004). Temporal structure of the fast convective flow in the plasma sheet: Comparison between observations and two-fluid simulations. *Journal of Geophysical Research*, *109*, A03210. https://doi.org/10.1029/2003JA010002

Panov, E. V., Nakamura, R., Baumjohann, W., Sergeev, V. A., Petrukovich, A. A., Angelopoulos, V., et al. (2010). Plasma sheet thickness during a bursty bulk flow reversal. *Journal of Geophysical Research*, *115*, A05213. https://doi.org/10.1029/2009JA014743

Runov, A., Angelopoulos, V., Gabrielse, C., Liu, J., Turner, D. L., & Zhou, X.-Z. (2015). Average thermodynamic and spectral properties of plasma in and around dipolarizing flux bundles. *Journal of Geophysical Research: Space Physics*, *120*, 4369–4383. https://doi.org/10.1002/2015JA021166

Runov, A., Angelopoulos, V., Sitnov, M. I., Sergeev, V. A., Bonnell, J., McFadden, J. P., et al. (2009). THEMIS observations of an earthward-propagating dipolarization front. *Geophysical Research Letters*, *36*, L14106. https://doi.org/10.1029/2009GL038980

Sergeev, V., Nishimura, Y., Kubyshkina, M., Angelopoulos, V., Nakamura, R., & Singer, H. (2012). Magnetospheric location of the equatorward prebreakup arc. *Journal of Geophysical Research*, *117*, A01212. https://doi.org/10.1029/2011JA017154

Sergeev, V. A., Chernyaev, I. A., Angelopoulos, V., Runov, A. V., & Nakamura, R. (2014). Stopping flow bursts and their role in the generation of the substorm current wedge. *Geophysical Research Letters*, *41*, 1106–1112. https://doi.org/10.1002/2014GL059309

Sergeev, V. A., Gordeev, E. I., Merkin, V. G., & Sitnov, M. I. (2018). Does a local B-minimum appear in the tail current sheet during a substorm growth phase? *Geophysical Research Letters*, *45*, 2566–2573. https://doi.org/10.1002/2018GL077183

Sergeev, V. A., Liou, K., Newell, P. T., Ohtani, S. I., Hairston, M. R., & Rich, F. (2004). Auroral streamers: Characteristics of associated precipitation, convection and field-aligned currents. *Annales Geophysicae*, *22*, 537–548. https://doi.org/10.5194/angeo-22-537-2004

Sergeev, V. A., Sazhina, E. M., Tsyganenko, N. A., Lundblad, J. A., & Soraas, F. (1983). Pitch-angle scattering of energetic protons in the magnetotail current sheet as the dominant source of their isotropic precipitation into the nightside ionosphere. *Planetary and Space Science*, *31*, 1147–1155. https://doi.org/10.1016/0032-0633(83)90103-4

Sergeev, V. A., Tsyganenko, N. A., Angelopoulos, V., Runov, A. V., & Singer, H. J. (2018). Magnetotail configuration during a steady convection event as observed by low-altitude and magnetospheric spacecraft. *Journal of Geophysical Research: Space Physics*, *123*, 8390–8406. https://doi.org/10.1029/2018JA025867

Silin, I., Toffoletto, F., Wolf, R., & Sazykin, S. Y. (2013). *Calculation of magnetospheric equilibria and evolution of plasma bubbles with a new finite-volume MHD/magnetofriction code. American Geophysical Union, Fall Meeting 2013*. SM51B-2176.

Sorathia, K. A., Ukhorskiy, A. Y., Merkin, V. G., Fennell, J. F., & Claudepierre, S. G. (2018). Modeling the depletion and recovery of the outer radiation belt during a geomagnetic storm: Combined MHD and test particle simulations. *Journal of Geophysical Research: Space Physics*, *123*, 5590–5609. https://doi.org/10.1029/2018ja025506

Tsyganenko, N. A. (1989). A magnetospheric magnetic field model with a warped tail current sheet. *Planetary and Space Science*, *37*(1), 5–20. https://doi.org/10.1016/0032-0633(89)90066-4

Tsyganenko, N. A., & Mukai, T. (2003). Tail plasma sheet models derived from Geotail particle data. *Journal of Geophysical Research*, *108*(A3), 1136. https://doi.org/10.1029/2002JA009707

Ukhorskiy, A. Y., Sorathia, K. A., Merkin, V. G., Sitnov, M. I., Mitchell, D. G., & Gkioulidou, M. (2018). Ion trapping and acceleration at dipolarization fronts: High-resolution MHD and test-particle simulations. *Journal of Geophysical Research: Space Physics*, *123*, 5580–5589. https://doi.org/10.1029/2018JA025370

Wang, C.-P., Zaharia, S. G., Lyons, L. R., & Angelopoulos, V. (2012). Spatial distributions of ion pitch angle anisotropy in the near-Earth magnetosphere and tail plasma sheet. *Journal of Geophysical Research: Space Physics*, *118*, 244–255. https://doi.org/10.1029/2012JA018275

Wiltberger, M., Merkin, V., Lyon, J. G., & Ohtani, S. (2015). High-resolution global magnetohydrodynamic simulation of bursty bulk flows. *Journal of Geophysical Research*, *120*, 4555–4566. https://doi.org/10.1002/2015JA021080

Yang, J., Toffoletto, F. R., & Wolf, R. A. (2014). RCM-E simulation of a thin arc preceded by a north-south-aligned auroral streamer. *Geophysical Research Letters*, *41*, 2695–2701. https://doi.org/10.1002/2014GL059840

Yang, J., Toffoletto, F. R., Wolf, R. A., & Sazykin, S. (2011). RCM-E simulation of ion acceleration during an idealized plasma sheet bubble injection. *Journal of Geophysical Research*, *116*, A05207. https://doi.org/10.1029/2010JA016346

Yang, J., Toffoletto, F. R., Wolf, R. A., & Sazykin, S. (2015). On the contribution of plasma sheet bubbles to the storm time ring current. *Journal of Geophysical Research: Space Physics*, *120*, 7416–7432. https://doi.org/10.1002/2015JA021398

Yang, J., Wolf, R. A., Toffoletto, F. R., & Sazykin, S. (2013). RCM-E simulation of substorm growth phase arc associated with large-scale adiabatic convection. *Geophysical Research Letters*, *40*, 6017–6022. https://doi.org/10.1002/2013GL058253

Yang, J., Wolf, R. A., Toffoletto, F. R., Sazykin, S., Wang, W., & Cui, J. (2019). The inertialized rice convection model. *Journal of Geophysical Research: Space Physics*, *124*, 10294–10317. https://doi.org/10.1029/2019JA026811

Zesta, E., Donovan, E., Lyons, L., Enno, G., Murphree, J. S., & Cogger, L. (2002). Two-dimensional structure of auroral poleward boundary intensifications. *Journal of Geophysical Research*, *107*(A11), 1350. https://doi.org/10.1029/2001JA000260

Zesta, E., Lyons, L., Wang, C.-P., Donovan, E., Frey, H., & Nagai, T. (2006). Auroral poleward boundary intensifications (PBIs): Their two-dimensional structure and associated dynamics in the plasma sheet. *Journal of Geophysical Research*, *111*, A05201. https://doi.org/10.1029/2004JA010640

Zhang, J.-C., Wolf, R. A., Erickson, G. M., Spiro, R. W., Toffoletto, F. R., & Yang, J. (2009). Rice Convection Model simulation of the substorm-associated injection of an observed bubble into the inner magnetosphere: 1. Magnetic field and other inputs. *Journal of Geophysical Research*, *114*, A08218. https://doi.org/10.1029/2009JA014130